Effect of Reinforcement on the Aging Response of Cast 6061 Al-Al_2O_3 Particulate Composites

I. DUTTA, S.M. ALLEN, and J.L. HAFLEY

The effect of 10 and 15 vol pct alumina particulate addition on the age hardening behavior of cast 6061 Al-matrix composites was studied using microhardness, electrical resistivity, differential scanning calorimetry, and transmission electron microscopy (TEM). It was found that the kinetics of precipitation in the matrix alloy are significantly accelerated due to the presence of reinforcements. This acceleration is attributable to the decrease in incubation time required for nucleation and the increase in solute diffusivity and hence precipitate growth rate resulting from the increase in the matrix dislocation density due to coefficient of thermal expansion (CTE) mismatch between the matrix and the reinforcements. The relative amounts of the various phases were also observed to be affected by reinforcement addition. Increasing reinforcement content decreased the volume fractions of the β' and β precipitates while increasing the volume fraction of the GP-I zones. The volume fraction of silicon clusters (which are the precursors to GP zones in 6061 Al) formed during postsolution treatment aging was found to decrease with increasing reinforcement addition. The above effects have been discussed with respect to the associated mechanisms, and plausible explanations have been offered.

I. INTRODUCTION

DISCONTINUOUSLY reinforced metal-matrix composites (MMCs) with precipitation hardenable matrices are known to age considerably faster than the unreinforced matrix alloy.[1–7] When discontinuous MMCs reinforced with ceramic particulates or whiskers are quenched from the solutionizing temperature, a high dislocation density is produced in the matrix due to differential thermal contraction of the matrix and the reinforcements.[1–3,6–10] Transmission electron microscopy (TEM) of SiC whisker-reinforced 2124 Al has shown that the matrix dislocations reduce the incubation time for heterogeneous nucleation of the strengthening precipitates, thereby accelerating the aging kinetics of the composite.[6] A theoretical analysis of precipitation kinetics in 6061 Al-SiC_w MMCs coupled with some experimental evidence suggested that the matrix dislocations may also enhance precipitate growth rate by serving as short circuit paths for solute diffusion.[11] In addition, the elastic strain field induced in the matrix by the presence of reinforcements can lead to enhanced matrix diffusivity and hence accelerated precipitation kinetics for composites with relatively low matrix dislocation density and/or large reinforcement particle size.[5] Detailed differential scanning calorimetry (DSC) studies have established that the addition of SiC to aluminum alloys does not alter the precipitation sequence of the matrix alloy, although both precipitation and dissolution kinetics are altered and some normally quench-insensitive materials, such as 6061 Al, become quench sensitive.[7] Studies of discontinuous δ-alumina fiber-reinforced Al-matrix composites have shown that the level of hardening obtained *via* aging in the composite is less than that in the unreinforced matrix alloy, attributable to the decreased vacancy concentration in the MMC.[12]

Most of the currently available literature on accelerated aging in metal-matrix composites is based on powder metallurgy (P/M) processed materials.[1,5–7,11] To date, no systematic investigation of the aging response of cast Al_2O_3 particulate reinforced aluminum-matrix composites has been reported. Cast SiC-aluminum composites were recently shown to exhibit accelerated aging due to the enhanced matrix dislocation density.[13] Since the coefficient of thermal expansion (CTE) of aluminum ($\sim 23 \times 10^{-6}$/K) is closer to the CTE of Al_2O_3 ($\sim 8 \times 10^{-6}$/K) than that of SiC ($\sim 3 \times 10^{-6}$/K), the thermal plastic strain (and hence the dislocation density) generated in the matrix during quenching from the solutionizing temperature is expected to be considerably less for Al_2O_3-Al composites than for SiC-Al. In addition, recent DSC studies have revealed that the kinetics of aging in cast materials are considerably slower than those observed in P/M processed materials.[7] Based on the above, the kinetics of precipitation in cast particulate Al_2O_3-Al composites may be expected to be considerably different from those observed in both powder metallurgy and cast SiC-Al composites.

The purpose of this article is to document the effect of alumina particulate reinforcement on the aging response of a cast 6061 Al-matrix composite. Changes in microhardness of the MMC matrix have been monitored as functions of aging time and reinforcement volume fraction. *In situ* resistivity measurements during aging, coupled with TEM, were conducted to characterize the sequence of precipitate evolution in the matrix alloy. A DSC investigation was also undertaken to observe the effect of reinforcements on each step in the precipitation sequence of 6061 Al.

I. DUTTA, Assistant Professor, is with the Department of Mechanical Engineering, Naval Postgraduate School, Monterey, CA 93943. S.M. ALLEN, Lt. Commander, United States Navy, formerly a Graduate Student, Naval Postgraduate School, is at Navsurfpac Naval Station, San Diego, CA. J.L. HAFLEY, Lieutenant, United States Navy, formerly a Graduate Student, Naval Postgraduate School, is at the U.S. Naval Station, Langley, VA.

Manuscript submitted November 26, 1990.

II. EXPERIMENTAL PROCEDURE

The metal-matrix composites used in this work were commercial aluminum alloy 6061 reinforced with 10 and 15 vol pct Al_2O_3 particles. The materials were fabricated by Duralcan Inc., San Diego, CA, using a proprietary casting technique. After casting, the material was hot-extruded to homogenize the microstructure. The alumina reinforcement particles, which had aspect ratios of about one, had irregular shapes and ranged in size from about 0.5 to 25 μm. For comparison, unreinforced commercial 6061 Al was obtained from ALCOA, Pittsburgh, PA, in the cast and wrought form and was used as a control material.

Microhardness measurements were conducted using a Buehler Micromet Tester equipped with a Vickers diamond pyramid indentor. Samples measuring 0.02 × 0.01 × 0.004 m were cut from the as-received stocks and were polished to a 1 μm finish. They were then solutionized at 813 K for 1.5 hours in a purified argon atmosphere and quenched in ice water at 273 K. Subsequently, the samples were aged at 473 K for various lengths of time and quenched to 273 K before hardness measurements were taken. Any interim storage before hardness testing was done in a freezer at 276 K. A minimum of seven hardness readings were taken for each composite sample with care being taken to avoid contact between the indentor and the reinforcement particles.

For the resistivity measurements, 0.115 × 0.038 × 0.018 m samples were machined from the as-received billets of the composite and the control alloy. Each sample was solutionized in argon atmosphere at 813 K and quenched to 273 K. Immediately thereafter, the sample was aged at either 293 ± 0.1 K or 473 ± 0.1 K and the electrical resistivity of the sample was monitored *in situ* using a standard four-point probe technique. The resistivity (ρ) *vs* time (t) data obtained from the tests were later converted into relative resistivity change ($\Delta\rho/\rho$) *vs* t to eliminate any effect of contact resistance. Each test was repeated at least twice to ensure reproducibility.

In order to relate change in ρ to the phase transformations occurring in the matrix, thin foils of the monolith and the 15 vol pct Al_2O_3 MMC were examined using a transmission electron microscope. The 0.003 m diameter disks were cut from the as-received stocks by electric discharge machining and were then ground mechanically to a thickness of about 25 μm using a TEM disc grinder. The samples were wrapped in aluminum foil, solutionized in inert atmosphere at 813 K for 1.5 hours, and quenched in ice water. They were then aged immediately for various lengths of time at either 293 or 473 K, quenched in ice water, and thinned to electron transparency. The unreinforced samples were thinned by electropolishing in a solution of 3 pct perchloric acid, 62 pct ethanol, and 35 pct butoxy-ethanol at 233 K using twin jets at a voltage of 18 V and a current of 30 mA. The composite samples were thinned in two steps. First, the disks were electropolished for 3 to 5 seconds using the above procedure to remove any deformation zone left over from the polishing step. The samples were then successively rinsed in water and high-purity ethanol and dried. In the second stage, the MMC disks were thinned using a GATAN duo-ion mill equipped with a liquid nitrogen cold stage at an accelerating voltage of 5 kV, a gun current of 1 mA, and a specimen to ion beam inclination of 12 deg. The final ion-thinning step, which lasted a maximum of 4 hours, was required to thin the alumina particles somewhat so that they would not fall out when a hole was obtained through the foil. Prior *in situ* ion-thinning experiments of aluminum alloys have shown that dislocation arrangements and microstructures are not altered by ion milling, although a limited number of point defects may be introduced in the foil.[14] All samples were examined using a JEOL 100CX TEM at an accelerating voltage of 120 kV. Any storage between preparation and observation was done at the liquid nitrogen temperature. Samples in the solutionized and quenched state and those aged for short times or at low temperatures were examined immediately after preparation to avoid storage in liquid nitrogen.

For the DSC experiments, 0.0015-m-thick disks of 0.0055-m diameter were machined from the as-received MMC and monolithic stocks by electric discharge machining. The disks were solutionized at 813 K for 1.5 hours in argon atmosphere and quenched in ice water at 273 K. They were then analyzed immediately in a PERKIN-ELMER* 2C DSC from 273 through 833 K using a heating rate of 10 K/min. In addition to the solutionized and quenched samples, samples preaged for 1.5 hours at 298 and 313 K were also analyzed. The heat flow data from each run were converted to heat capacity (C_p) by using a previously established calibration factor. The C_p *vs* temperature (T) data were subsequently transformed into differential heat capacity (ΔC_p) *vs* T by subtracting a baseline representing the C_p of the alloy with its existing precipitates. The baseline was approximated by scanning a sample aged for 72 hours at 473 K (overaged) from 273 to 800 K (the start of the equilibrium-phase dissolution peak) and extrapolating the plot to 833 K.[16]

*PERKIN-ELMER is a trademark of Perkin-Elmer Physical Electronics, Eden Prairie, MN.

III. EXPERIMENTAL RESULTS

A. *Dislocation Density Analysis by TEM*

The matrix dislocation densities ($\rho_\perp$) of the monolithic 6061 Al and the 10 and 15 vol pct Al_2O_3 reinforced composites were measured using the line intercept method.[15] The matrix dislocation density was determined from five micrographs of each of two separate samples of each material, and the mean value of $\rho_\perp$ and its standard deviation were calculated. Typical dislocation structures of the solutionized and as-quenched control alloy and the two composites are shown in Figures 1(a) through (c). The mean dislocation density of the solutionized and as-quenched control alloy was found to be 3.1×10^{10} m^{-2} with a standard deviation of 3.6×10^{10} m^{-2}. The dislocation density in the 10 vol pct Al_2O_3 composite was found to be 4.5×10^{12} m^{-2} ± 2.0×10^{12} m^{-2}, while for the 15 vol pct Al_2O_3 composite it was 7.3×10^{12} m^{-2} ± 1.8×10^{12} m^{-2}. In general,

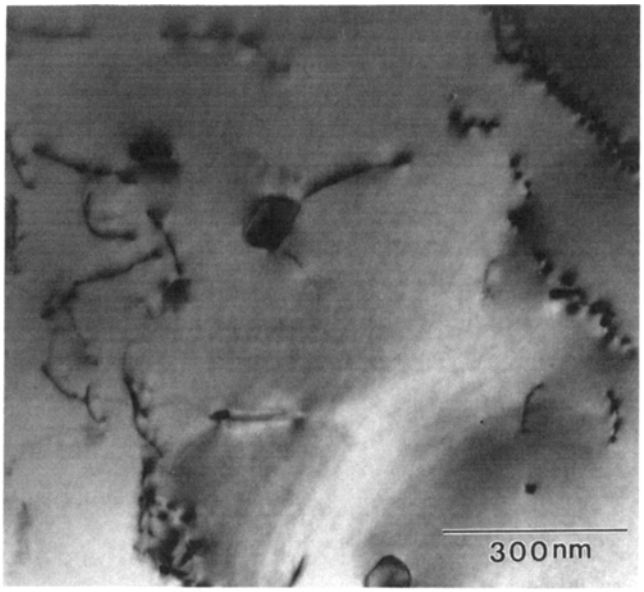

(*a*)

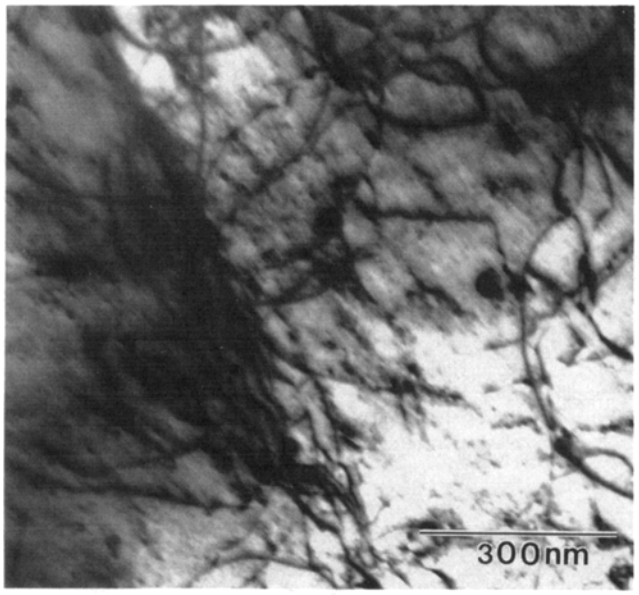

(*b*)

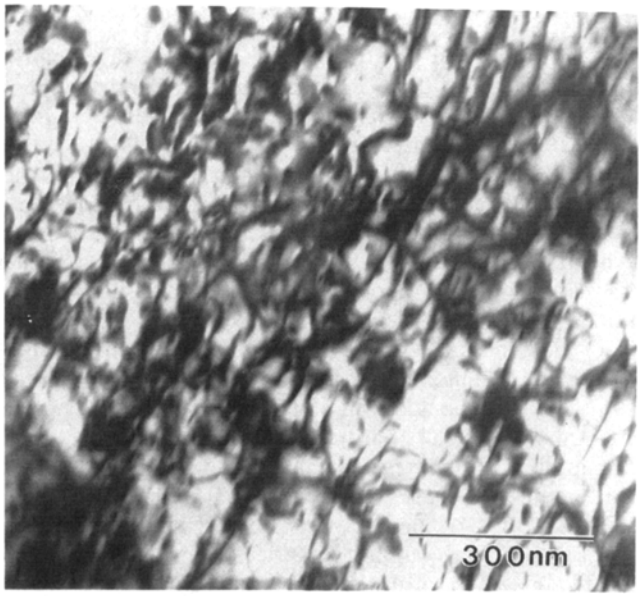

(*c*)

Fig. 1—Representative dislocation structures of the (*a*) solutionized and quenched control alloy, (*b*) 10 vol pct Al_2O_3 composite, and (*c*) 15 vol pct Al_2O_3 composite in areas away from reinforcement particles. It is clear that the dislocation densities in the composite matrices are much higher than in the monolithic alloy.

the composites were fairly evenly dislocated throughout, as opposed to the control alloy which showed dense random dislocation arrays in some areas, evolving low-angle grain boundaries in others, and very low dislocation density in still other areas. However, as evident from the above numbers, the mean dislocation density in the composite matrices was significantly greater than that in the control alloy. It is apparent that while the increase in reinforcement volume percent from 0 to 10 increases the matrix dislocation density by about two orders of magnitude, a further increase from 10 to 15 leads to comparatively little additional increase in $\rho_{\perp}$.

B. *Microhardness*

Figure 2 shows the microhardness variation as a function of aging time at 473 K for the monolithic 6061 Al as well as the 10 and 15 vol pct Al_2O_3 MMCs. It is evident that there is considerable scatter in the microhardness of the composites. Although care was exercised to record the data from the matrix without indenting any reinforcement particle, occasional occurrence of subsurface particles caused the hardness to vary appreciably. In addition, the reinforcement distribution in the composites was rather inhomogeneous, with clusters of alumina particles separated by regions of

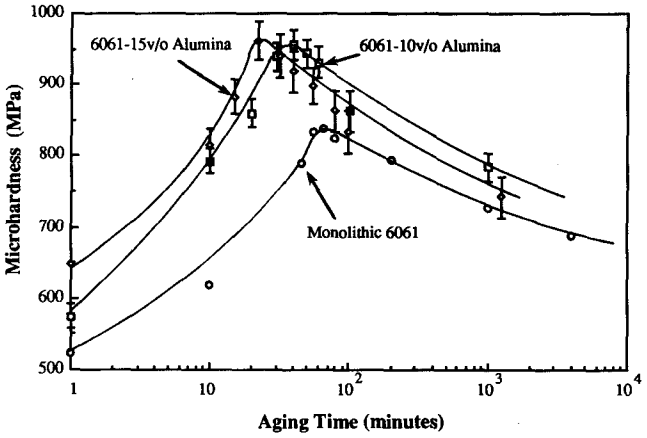

Fig. 2—Microhardness as a function of aging time at 473 K for the control alloy and the composites with 10 and 15 vol pct Al_2O_3 particulates. The addition of alumina reinforcements is observed to decrease the time to peak hardness. The composites exhibit considerable scatter in the hardness data, suggesting that the matrix microhardness is strongly dependent on the distance from the reinforcements.

reinforcement-free matrix. This caused the matrix microhardness of the composites to be strongly dependent upon distance from reinforcement clusters, resulting in the observed scatter.

Three features of Figure 2 are noteworthy. First, the solutionized and as-quenched matrix microhardness increases with increasing alumina additions. This suggests that the enhanced dislocation density in the composite matrices contributes appreciably to the increased strength of these materials. Second, the addition of 10 vol pct Al_2O_3 decreases the time to peak hardness from approximately 65 minutes in the monolith to about 40 minutes in the MMC. The addition of 15 vol pct Al_2O_3 decreases the time to peak hardness still further, to about 25 minutes. This suggests that the addition of alumina reinforcements causes considerable acceleration in the aging kinetics of the matrix alloy. Third, the microhardnesses of the composite matrices start out higher than the microhardness of the monolith and remain higher until peak age. Beyond peak age, little difference is observed between the microhardness of the monolith and the composites. This suggests that during the early stages of aging, both the matrix dislocation density and the precipitation of metastable phases contribute to the overall matrix hardness. As the matrix overages, the influence of matrix dislocations becomes less pronounced, probably because the relatively high aging temperature allows some dislocation recovery at the longer aging times. Accelerated precipitate growth, resulting in quick overaging of the composite matrices, might also be partly responsible for the comparable hardness values observed in the monolith and the composites beyond peak age. Since little difference is noted between the peak hardnesses of the 10 and 15 vol pct Al_2O_3 composites, it can be inferred that even in the peak-aged condition, some strain accommodation has occurred in the composites due to recovery, thereby obfuscating any evidence of the marginally higher dislocation density in the 15 Al_2O_3 vol pct MMC.

C. *In Situ Resistivity and TEM*

1. *Precipitation processes accompanying resistivity changes in 6061 Al*

The variation of electrical resistivity with time at an aging temperature of 473 K is shown in Figure 3 for monolithic 6061 Al. Figure 3 suggests that the resistivity of 6061 Al changes in three stages concurrent with aging: stage I, representing the rapid initial rise in resistivity; stage II, during which the resistivity remains essentially constant with time; and stage III, where the resistivity decreases with aging time.

Figure 4 shows the bright-field (BF) TEM micrograph of the unreinforced 6061 Al sample aged for 50 seconds at 473 K. A high density of very tiny (~1 to 2 nm) precipitates are observed. The formation of these precipitates was accompanied by an increase in microhardness from about 500 to 530 MPa. These precipitates

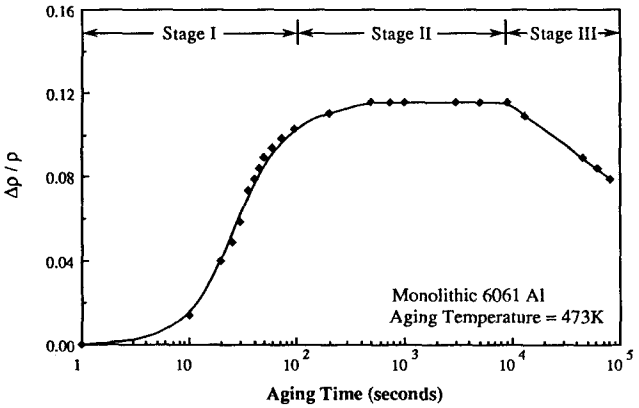

Fig. 3—The variation of electrical resistivity with time at an aging temperature of 473 K for the monolithic 6061 Al. Three stages are evident. The resistivity increases rapidly during stage I, remains relatively constant during stage II and decreases during stage III.

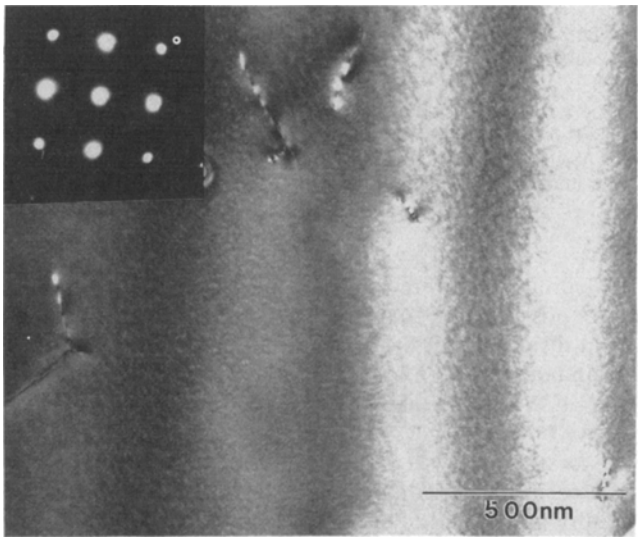

Fig. 4—BF TEM micrograph of the monolithic control alloy aged for 50 seconds at 473 K, showing a high density of tiny silicon clusters. The corresponding SADP of the 001 pole shows no additional features which are representative of the clusters.

were previously identified as coherent silicon clusters.[16] These precipitates form quickly at quenched-in vacancy loops even at relatively low aging temperatures and are known to be precursors for GP zones in Al-Mg-Si alloys.[17,18,19] The microstructure of the monolithic alloy aged for 100 seconds at 473 K is shown in Figure 5. Coherent precipitates appearing as dots about 3 to 4 nm in diameter are observed. These near-spherical precipitates, which have been observed earlier by other investigators,[20,21] were recently identified to be GP-I zones.[16] The accompanying selected area diffraction pattern (SADP) reveals very faint $\langle 100 \rangle_{Al}$ streaks, suggesting that in addition to the near spherical GP-I zones, a limited number of tiny, needle-shaped precipitates situated along $\langle 100 \rangle_{Al}$ are also present after aging for 100 seconds at 473 K. These needle-shaped precipitates are more clearly visible in Figure 6, which shows the BF micrograph of a sample aged for 2000 seconds at 473 K. The needles, which are approximately 15- to 20-nm long and 5 nm in diameter, are seen to be oriented along $\langle 100 \rangle_{Al}$, resulting in the prominent streaks in the SADP. These needle-like precipitates represent the β'' phase (or GP-II zones)[16,22–25] which forms competitively with GP-I zones from silicon clusters.[16] Figure 7 shows the TEM micrograph of a sample aged for 50,000 seconds at 473 K. Here, the needles are seen to have coarsened into rods which are approximately 150- to 200-nm long and about 100 Å in diameter. These coarse rod-like precipitates are the metastable β' phase, which ultimately transform into the equilibrium β-Mg_2Si precipitates by further lateral coarsening.[16,20–24]

From the above, it is clear that stage I in Figure 3, which represents the quick initial rise in resistivity until about 150 seconds, is associated with the formation of coherent silicon clusters at quenched-in vacancy loops and their subsequent transformation to GP-I zones. The matrix strain associated with the formation of silicon clusters and GP-I zones is primarily responsible for the rise in resistivity. In stage II, needle-like GP-II zones or β'' grow from the pre-existing silicon clusters and GP-I zones. Concurrent with the formation of the needle-like precipitates, a large matrix strain develops perpendicular to the needle axes.[16,24] While the transformation-induced strain field tends to increase the resistivity, continued solute depletion from the matrix due to precipitate growth tends to decrease it, keeping the overall resistivity constant with time. As the precipitates coarsen into the semicoherent β' and eventually the incoherent β, the matrix strain decreases, as does the precipitate density. This decrease in strain, coupled with concurrent reduction in the matrix solute content, results in a net drop of resistivity in stage III.

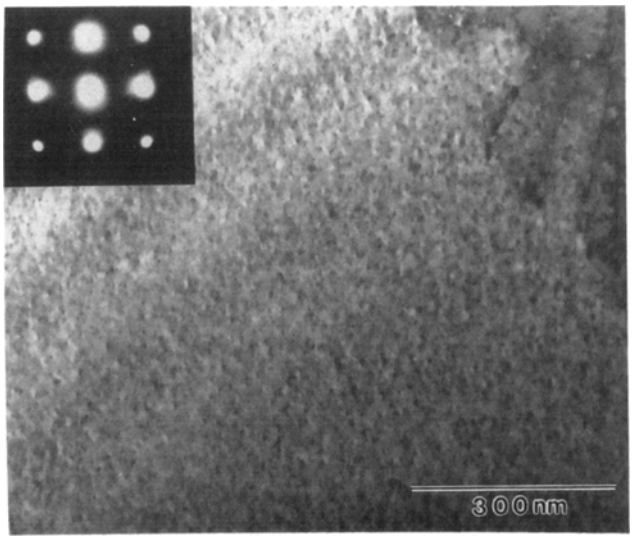

Fig. 5—BF TEM micrograph of the control alloy aged for 100 seconds at 473 K, showing near-spherical GP-I zones. The SADP shows no additional features representative of the GP-I zones. The very faint ⟨100⟩ streaks observed suggest that a limited amount of tiny needle-shaped GP-II zones (β'') is also present.

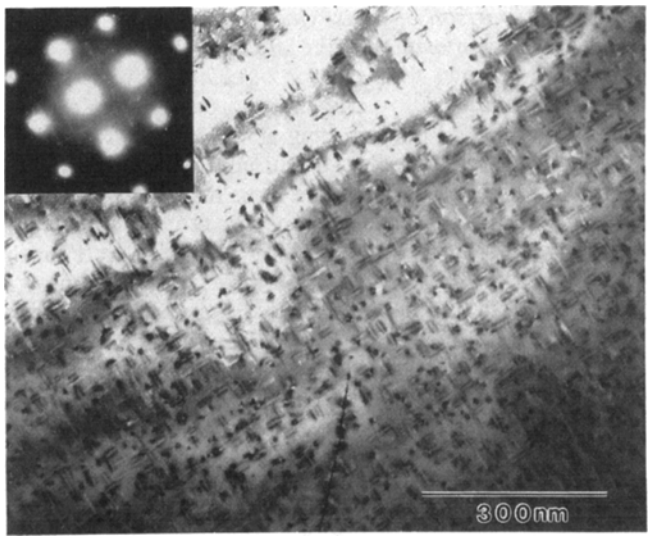

Fig. 6—BF micrograph of the control alloy aged for 2000 seconds at 473 K, revealing fine needle-like GP-II zones. These zones cause the prominent ⟨100⟩ streaking observed in the SADP.

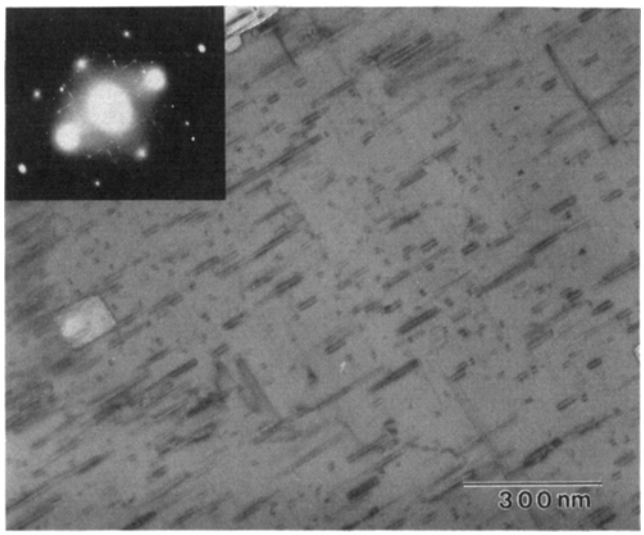

Fig. 7—BF TEM micrograph and the corresponding SADP of monolithic 6061 Al aged for 50,000 seconds at 473 K, showing rod-like β' precipitates.

2. *Comparison of resistivity changes in the monolith and the composites during aging*

Figure 8 shows the variation of electrical resistivity of the unreinforced alloy and the two composites (10 and 15 vol pct Al_2O_3) during aging at 473 K. Relatively little difference is observed in the durations of stage I of the resistivity change between the three materials. However, stage II for the composites is observed to be considerably shorter than that for the monolith. While stage II for the unreinforced alloy extends to about 10,000 seconds, in the composites, it extends to only about 300 to 400 seconds. Figure 9 shows the precipitate microstructure in the 15 vol pct MMC after 300 seconds of aging at 473 K. Coarse precipitate rods (β'), about 20 nm in diameter, are observed. This corresponds roughly to the microstructure of the control alloy aged for about 60,000 seconds at the same temperature. The above indicates that the formation of the needle-like β'' precipitates and their eventual coarsening into β' rods are substantially accelerated in the composites. Since no new nucleation is necessary for the transformation of the silicon clusters into β'' and the subsequent formation of β', it can be inferred that growth is significantly accelerated in the MMCs.

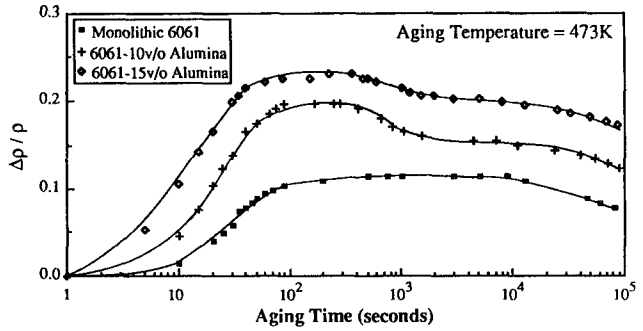

Fig. 8—The variation of electrical resistivity with aging time at 473 K for monolithic 6061 Al and the composites with 10 and 15 vol pct Al_2O_3 particulates. It is observed that the addition of reinforcement particles shortens stage II significantly.

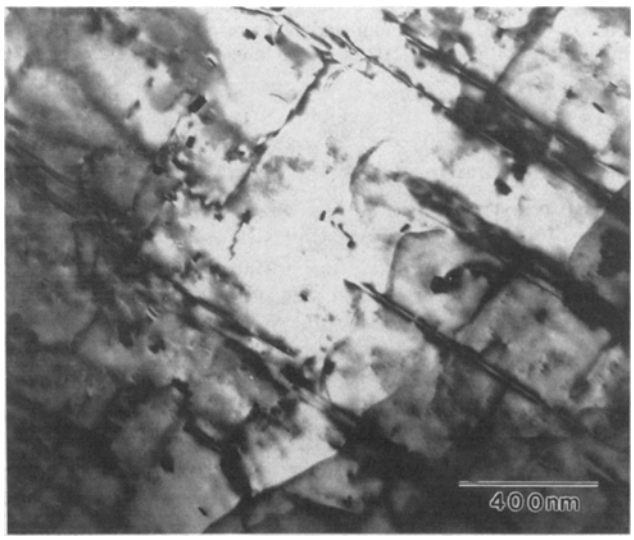

Fig. 9—The matrix microstructure of the 15 vol pct Al_2O_3 composite aged for 300 seconds at 473 K, showing coarse β' precipitate rods.

The formation of transition precipitates (β'', β') in Al-Mg-Si alloys occurs due to the precipitation of magnesium and silicon atoms from the solid solution on preexisting nuclei,[18] which could be either silicon clusters or silicon clusters which have already grown into GP-I zones, as discussed earlier. Since magnesium has an atomic diameter of 0.3196 nm *vs* 0.2351 nm for Si, the diffusivity of Mg in Al is less than that of Si in Al ($D_{Si} \sim 5 \times 10^{-15}$ m^2/s; $D_{Mg} \sim 6.5 \times 10^{-15}$ m^2/s at 673 K[25]). In addition, the Mg-Si bond is characterized by a large interaction energy, suggesting that the formation of the transition precipitates is not interface-jump controlled, but rather, Mg-diffusion controlled. Therefore, any acceleration of β'' formation and the coarsening thereof to β' must result from increased Mg diffusivity in Al. It is thus evident that the presence of reinforcements increases the apparent diffusivity (D_{app}) of magnesium by increasing the matrix dislocation density. The apparent diffusivity, which depends both on lattice diffusivity and pipe diffusivity, increases linearly with the matrix dislocation density.[11] The increase in dislocation density from 3.1×10^{10} to 4.5×10^{12} m^{-2} increases D_{app} significantly, leading to the substantial shortening of stage II observed in the 10 vol pct alumina MMC relative to the unreinforced alloy. A further increase of $\rho_\perp$ to 7.3×10^{12} m^{-2} in the 15 vol pct MMC results in a comparatively insignificant increase in the Mg diffusivity, as evident from the nearly equal stage II in the two composites.

Figure 10 shows the variation of electrical resistivity during aging at 293 K of the control alloy and the 10 and 15 vol pct Al_2O_3 composites. Essentially no change in resistivity is observed in the control monolithic alloy for the first 3000 seconds. After that, the resistivity rises rapidly until about 15,000 seconds, followed by a slower rise. The 10 vol pct composite shows a similar trend, although the start of resistivity rise is accelerated to about 800 seconds. The subsequent slower rise of resistivity is also accelerated relative to the monolith to approximately 9000 seconds. In contrast to the behavior exhibited by the control alloy and the 10 vol pct composite,

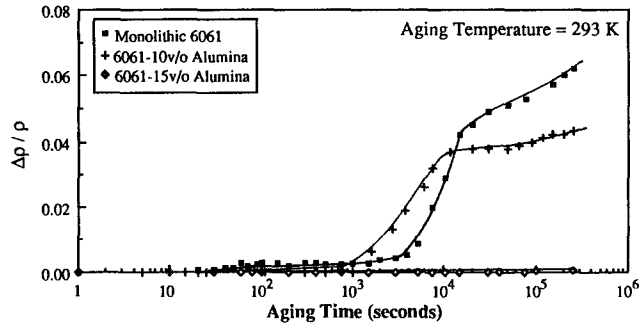

Fig. 10—The variation of electrical resistivity with aging time at 293 K for monolithic 6061 Al and the composites with 10 and 15 vol pct Al_2O_3 particulates. The rise in resistivity of the monolithic alloy and the 10 vol pct MMC is associated with the nucleation and growth of silicon clusters. No change in the resistivity occurs in the 15 vol pct composite, since no nucleation of silicon clusters takes place during aging at 293 K.

the 15 vol pct composite shows no change in resistivity at 293 K for 3×10^5 seconds.

Transmission electron microscopy observation of the monolith and the 10 vol pct MMC aged for various times showed that the resistivity change concurrent with aging at 293 K is associated with the nucleation and growth of silicon clusters. The initial period over which there is no change in resistivity is representative of the incubation time required for nucleation. During the subsequent rapid rise in resistivity, prolific nucleation occurs in the matrix. As site saturation occurs with increasing aging time, little additional nucleation takes place and further precipitation of silicon becomes growth dominated, concomitant with the slower rise in resistivity. From the above, it is evident that the nucleation of silicon clusters is accelerated in the 10 vol pct composite due to a reduction of the incubation time. A similar effect has been observed earlier[6] on adding SiC whisker reinforcements to aluminum alloy 2124. Little difference in the durations of the nucleation-dominated stage of the monolith and the 10 vol pct MMC is observed in Figure 10, suggesting that the nucleation rate *per se* is not accelerated appreciably. The absence of any significant resistivity change in the 15 vol pct MMC is attributable to the fact that silicon clusters were formed almost instantaneously on quenching, and the postquench aging at 293 K resulted in no additional nucleation of Si clusters and little additional growth. This is confirmed by the BF TEM micrograph of the solutionized and as-quenched 15 vol pct composite, showing silicon clusters densely populating the entire matrix (Figure 11). The clusters, the size of which can only be estimated from the size of the strain field around them, are observed to be relatively coarse (~2 to 3 nm), suggesting that a significant degree of growth has already occurred. The duration of the resistivity test (~3 days) was not sufficient to cause the formation of GP-I zones (and the concomitant rise in resistivity), since it requires magnesium diffusion and is therefore a very slow process at 293 K.

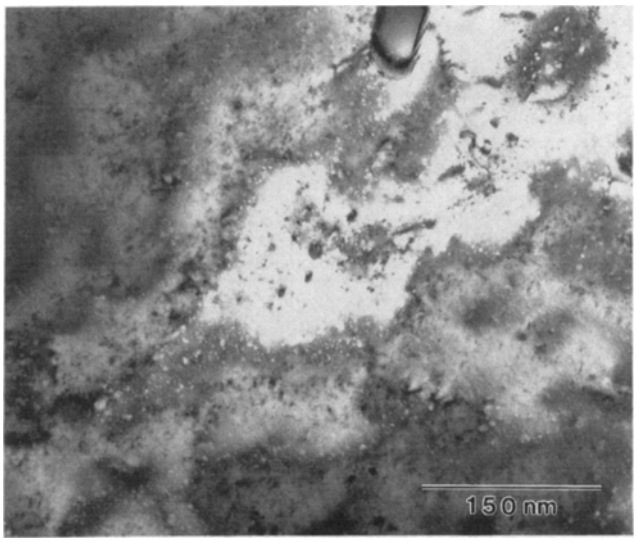

Fig. 11—BF TEM micrograph of the solutionized and as-quenched 15 vol pct Al_2O_3 composite matrix, showing relatively coarse silicon clusters which formed during quenching.

D. *Differential Scanning Calorimetry*

Figure 12 shows the DSC thermograms of the control alloy, the 10 vol pct Al_2O_3 composite, and the 15 vol pct Al_2O_3 composite after solutionizing and quenching. The matrix compositions of the monolith and the composite are listed in Table I. Four distinct exothermic peaks (corresponding to precipitate formation processes) and one endothermic dissolution peak are visible. Detailed TEM characterization of these peaks is reported elsewhere for the monolithic 6061 Al alloy.[15] The first exothermic peak, which occurs around 360 K, represents the formation of silicon clusters. The second and third partially overlapping exotherms, occurring between 460 and 610 K, represent the precipitation of the metastable transition phases. The second exotherm is actually an unresolved doublet[16] associated with the formation of near-spherical GP-I zones and needle-like GP-II zones or β''. The third exotherm represents the formation of rod-like β' precipitates, while the final exotherm, which occurs around 760 K, represents the formation of the equilibrium β platelets. The endotherm around 810 K is associated with the dissolution of the β phase.

Several effects of adding reinforcements are evident from Figure 12. First, the Si-cluster exotherm is seen to become smaller upon addition of 10 vol pct Al_2O_3 and disappear completely when the reinforcement volume percent is increased to 15. In Section III–C–2, it was found that silicon clusters form in the 15 vol pct MMC on quenching from the solutionizing temperature. No further Si precipitation occurs during the DSC scan, resulting in the disappearance of the peak. In the 10 vol pct MMC, some Si clustering occurs on quenching, although the majority of Si precipitates form during the scan. This reduces the area under the peak, which is proportional to the volume fraction of the precipitates forming during the scan. No effect of reinforcements is observed on the peak temperature associated with Si clustering.

Second, by comparing the convoluted GP-I/GP-II zone doublet (the second exothermic peak) for the control alloy and the 10 vol pct composite, it is apparent that the relative proportion of GP-I zones in the doublet is larger in

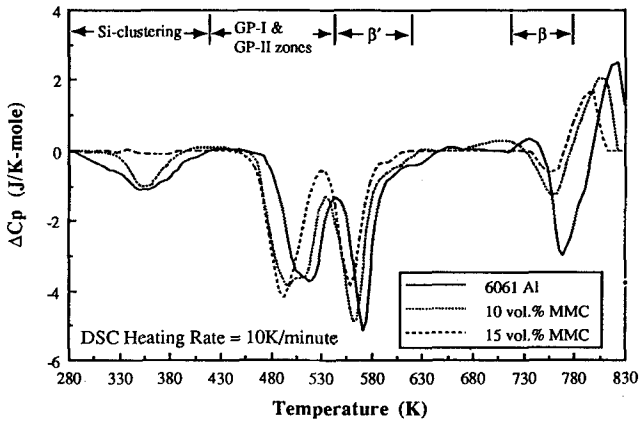

Fig. 12—DSC thermograms of the monolithic 6061 Al and the composites with 10 and 15 vol pct Al_2O_3 particulates in the solutionized and as-quenched condition. The final endotherm represents β-phase dissolution.

the composite than in the monolith. In the 15 vol pct composite, the GP-I zone and GP-II zone (β'') peaks overlap completely. However, it is evident that the GP-I zone phase is the predominant contributor to the unresolved doublet. This suggests that the relative proportion of GP-I zones to GP-II zones increases with increasing reinforcement volume fraction. The effect of reinforcements on the peak temperature of GP-I or GP-II zones is not readily quantifiable, although it appears that the peak temperatures decrease with increasing reinforcement content.

Third, it is evident from Figure 12 that the peak temperatures for both β' and β formation decrease with increasing alumina volume fraction, suggesting that the presence of reinforcements accelerates the kinetics of formation of these phases. Table II summarizes the peak temperatures associated with the formation of various phases in the monolith and the two composites. It is also observed in Figure 12 that the sizes of the β' and β formation peaks (which are proportional to the volume fractions of the respective phases that form during the scan) decrease with increasing reinforcement volume fraction. This is especially true for the β phase, the volume fraction of which decreases sharply with increasing alumina content. This suggests that the presence of alumina particulates suppresses the transformation of the GP zones to β' and β phases. It is well established that there is a strain field associated with the formation of GP zones in 6061 Al, which gets progressively relieved as the zones transform into the semicoherent β' and finally into the incoherent β.[16,24,26] When dislocations are available for precipitation, the coherent and semicoherent precipitates in Al-Mg-Si alloys orient themselves such that the direction of maximum strain coincides with the Burgers vector of the host dislocation, thereby reducing the associated strain energy.[27] In the composites, the high matrix dislocation density allows a predominant fraction of the precipitates to form at dislocations, thereby relieving part of the strain associated with the process. It is possible that this obviates the need to reduce strain energy by the usual coherent → semicoherent → incoherent transformation, explaining the smaller β' and β volume fractions observed in the composites.

Figure 13 illustrates the effect of preaging for 1.5 hours at 298 and 313 K on the Si-cluster formation peak of the 10 vol pct alumina composite. The response of the monolith to preaging was similar and is reported elsewhere.[16] It is seen that with greater preaging temperatures, the Si-cluster peak shifts to higher temperatures (T_p) while the heat of reaction (ΔH_R) associated with the peak decreases. The effect of preaging temperature on T_p and ΔH_R in the monolithic control alloy and the 10 vol pct composite is documented in Table III, which also lists the Arrhenius activation energy (E_a), activation entropy (ΔS_a), and free energy of activation (ΔG_a) associated with the formation of silicon clusters during the DSC scan. The values of E_a, ΔS_a, and ΔG_a were calculated using the absolute reaction rate theory,[28,29] approximating silicon clustering from the supersaturated solid solution as a first-order reaction. It is evident from Table III that with preaging at higher temperatures, the activation energy E_a increases while

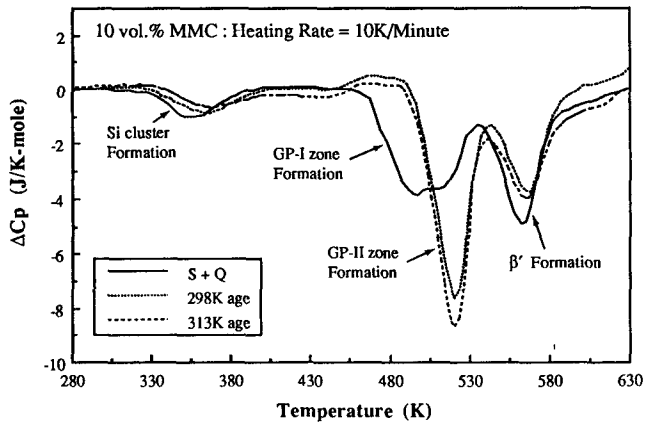

Fig. 13—DSC thermograms of the 10 vol pct Al_2O_3 containing composite in the solutionized and as-quenched state (S + Q) and after preaging for 1.5 hours at 298 and 313 K. The GP-I zone peak is observed to disappear on preaging, which also decreases the size of the Si-clustering peak and shifts it to higher temperatures.

Table I. Composition of the Control Alloy and the Composite Matrices in Weight Percent

	6061 Al	10 Vol Pct MMC	15 Vol Pct MMC
Silicon	0.63	0.67	0.62
Magnesium	0.85	0.66	0.60
Copper	0.24	0.26	0.22
Iron	0.45	0.26	0.24
Chromium	0.15	0.04	0.04
Manganese	0.11	0.03	0.03
Zinc	0.04	0.06	0.06
Titanium	0.04	0.03	0.03
Nickel	<0.005	0.006	0.006
Others	<0.15	—	—
Aluminum	bal.	bal.	bal.

Table II. Peak Temperatures (T_p) of DSC Exotherms

Precipitates	6061 Al	6061 Al-10 Vol Pct Alumina	6061 Al-15 Vol Pct Alumina
Si clusters	355 K	355 K	not present
GP-I zones	*	*	*
GP-II zones (β'')	*	*	*
β'	572 K	564 K	559 K
β	770 K	765 K	757 K

*Peak temperatures not discernible because of superposition.

the magnitude of the activation entropy ΔS_a decreases. The free energy of activation, ΔG_a, is found to increase with increasing preaging temperatures, suggesting that ΔG_a is controlled by the activation energy and not the entropy. Both the control alloy and the 10 vol pct MMC exhibit the same behavior. However, ΔH_R and, therefore, the volume fraction of silicon clusters formed during the DSC scan are considerably smaller in the 10 vol

Table III. Effects of Reinforcement Addition and Preaging on Precipitation

Material	T_p (K)	ΔH_R (J/mole)	E_a (kJ/mole)	ΔH_a (kJ/mole)	ΔS_a (J/K-mole)	ΔG_a (kJ/mole)
6061 Al Sol. + Que.	355	63	33.10 ± 7.5	30.14 ± 7.8	−204 ± 21	103.10 ±6.2
6061 Al 298 K Age	363	58	43.70 ±11.2	40.74 ±21.6	−174 ± 61	104.40 ±4.0
6061 Al 313 K Age	369	50	46.44 ±13.1	43.43 ±13.1	−172 ± 44	105.14 ±4.6
10 pct MMC Sol. + Que.	355	43	54.63 ±12.0	51.68 ±12.1	−143 ± 33	102.66 ± 4.3
10 pct MMC 298 K Age	365	39	59.66 ±14.3	55.62 ±14.5	−136 ± 40	104.80 ± 2.7
10 pct MMC 313 K Age	370	23	64.50 ±15.1	61.41 ±15.0	−117 ± 42	105.30 ±1.86

pct composite than in the monolith for each preaging condition. It is also observed that for each condition, E_a is appreciably larger for the composite than for the monolith while the magnitude of ΔS_a is smaller, rendering ΔG_a for both materials comparable.

In the monolithic alloy, nucleation of Si precipitates occurs primarily on quenched-in vacancy loops, the density of which decrease with higher preaging temperatures due to coalescence, growth, and possibly some annihilation. This decreases the number of available nucleation sites and the nucleation rate while increasing the incubation time, causing the Si-cluster peak to shift to higher temperatures during the scan. Higher preaging temperatures also result in some Si nucleation during preaging, thereby reducing ΔH_R and the volume fraction of Si formed during the DSC scan. Since the same trends are observed in the 10 vol pct composite, it can be inferred that a substantial fraction of the nucleation in the MMC occurs on the quenched-in vacancy loops, although as discussed earlier, the matrix dislocations also contribute significantly to the nucleation process. If only the matrix dislocations were responsible for nucleation in the MMC, the observed rise in peak temperature due to the reduction in vacancy loop density would not have occurred in the composite.

The smaller ΔH_R for the solutionized and as-quenched 10 vol pct composite relative to the control alloy can be attributed to the formation of some Si clusters in the MMC during the quench, leaving a smaller volume fraction to be formed during the DSC scan. Since the vacancy concentration in the composite is expected to be lower than that in the monolith (because the higher matrix dislocation density and the particulate-matrix interfaces in the MMC provide more annihilation sites for vacancies), the acceleration in the nucleation of Si clusters in the MMC must be due to the presence of matrix dislocations which act as sites for early nucleation. Therefore, it can be inferred that during quenching, some Si clustering occurs at the matrix dislocations which are already present. Additional clustering during aging occurs predominantly at the quenched-in vacancy loops present in the matrix.

As noted earlier, the overall activation energy for Si clustering (E_a), which incorporates the activation energies for both nucleation and growth, is considerably greater in the 10 vol pct composite than in the monolith for each condition. The term E_a represents the activation energy for silicon clustering during the DSC scan, *i.e.*, for clustering at vacancy loops. Since the composite matrix is expected to have a considerably lower density of vacancies than the monolith, the measured activation energies for both nucleation and growth in the composite are expected to be greater. This is because the reduced vacancy concentration in the composite matrix decreases the vacancy migration contribution to nucleation and growth while increasing the contribution of substitutional atom migration (which requires creation of vacancies and therefore has a larger activation energy), resulting in an increase in the measured value of E_a. However, as seen from Table III, the increase in E_a with reinforcement is accompanied by a decrease in the magnitude of ΔS_a, keeping ΔG_a and hence the peak temperature T_p unchanged.

Figure 13 also shows that the GP-I zone formation peak disappears on preaging, while the GP-II zone (β'') exotherm gets enlarged. This indicates that preaging supports the formation of GP-II zones directly from Si clusters without going through the intermediate GP-I zone. An identical behavior was observed in the monolithic 6061 Al alloy, and it was inferred that the formations of GP-I and GP-II zones from silicon clusters are parallel, competitive processes.[16] Preaging reduces the density of quenched-in vacancy clusters which act as nucleation sites for precipitates, as a result of which fewer, coarser vacancy-silicon clusters are formed on subsequent aging. These coarse silicon clusters apparently promote the formation of the needle-like GP-II zones (β'') in preference to the near-spherical GP-I zones which form only if the silicon clusters are very fine. Since the same behavior was observed in both the composite and the monolith, it can be inferred that the presence of reinforcements does not alter significantly the precipitation behavior following preaging, although as discussed earlier,

reinforcements can have an appreciable effect on the vacancy concentration of the matrix.

IV. DISCUSSION

From Section III, it is evident that the presence of alumina particulates significantly increases the matrix dislocation density of a 6061 Al matrix composite during quenching from the solutionizing temperature. The increased dislocation density results in a decrease of the incubation time required for silicon-cluster nucleation. The reduced incubation period leads to the formation of a significant amount of silicon clusters during the quenching process. The proportion of silicon clusters formed during the quench depends on the matrix dislocation density and hence the reinforcement volume fraction. Quenched-in vacancy loops act as additional sites for the nucleation of silicon clusters during subsequent aging, depending on the degree of clustering that has already occurred at the matrix dislocations during quenching and the concentration of excess solute available for further clustering. In the 10 vol pct Al_2O_3 composite, some of the silicon clustering occurs during quenching while the rest occurs during aging, while in the 15 vol pct Al_2O_3 composite, nearly all of the clustering occurs during quenching. Thus, the nucleation of precipitates in a 6061 Al matrix composite takes place on two different kinds of sites: (A) matrix dislocations generated as a result of the CTE difference between the matrix and the reinforcement and (B) quenched-in vacancy loops. A higher reinforcement content increases nucleation on the A site and decreases the concentration of the B sites, thereby decreasing the contribution of the B sites to the overall nucleation process.

During subsequent aging, magnesium atoms diffuse to and segregate at the already present silicon clusters, forming the transition phases (GPZ-I, β'', and β'). While the presence of a large number of matrix dislocations increases the pipe diffusion component of the apparent diffusivity, the lattice diffusion component decreases because of the smaller vacancy concentration in the highly dislocated matrix. At the usual aging temperatures (which are relatively low for aluminum alloys, *i.e.*, <473 K), pipe diffusion dominates and the overall diffusivity of magnesium increases with increasing matrix dislocation density and reinforcement volume fraction. This accelerates the precipitation process, the acceleration being more evident for precipitates with high magnesium content (*i.e.*, β' and β-Mg_2Si). This is supported by the abatement of stage II of the resistivity change with alumina addition during isothermal aging at 473 K as well as by the decrease in β' and β peak temperatures with increased reinforcement content during nonisothermal aging in the DSC. Thus, in addition to nucleation, precipitate growth is also accelerated due to the presence of alumina reinforcements.

Besides altering the kinetics of precipitation, the addition of alumina particulate reinforcements appears to alter the relative proportions of the various phases formed in the matrix alloy during aging. Reinforcements seem to stabilize the GP zones, thereby reducing the volume fractions of β' and β formed, especially at higher reinforcement contents. As discussed earlier, one reason for this effect might be dislocation-aided relief of the matrix strain associated with the early precipitates. Additionally, the diffusion of Mg and its subsequent incorporation into the reinforcement at the Al_2O_3-Al interface might also result in Mg depletion from the matrix, accounting for the reduced β' and β peak sizes. Magnesium incorporation into interfacial alumina to form $MgAl_2O_4$ has been observed in graphite fiber-reinforced 6061 Al composites.[30] Part of the reduction in the volume fractions of β' and β formed during the DSC scans might also stem from the reduced magnesium content in the composite matrices relative to the control monolithic alloy (Table I). However, it is unlikely that the relatively small difference in the magnesium contents of the 10 and 15 vol pct Al_2O_3 composites could be responsible for the entire difference in the β' and β peak sizes observed between the two materials in Figure 12. Reduction in the β' and β peak sizes due to reinforcement addition has also been observed in an earlier study on P/M processed SiC_w-6061 Al composites.[7] This decrease was attributed to the decrease in the density of quenched-in vacancies which are necessary for nucleation and for enhancing growth at low temperatures. This explanation, however, does not account for the substantial amount of early nucleation that occurs on the thermally generated matrix dislocations during the quenching process nor does it explain the increase in the volume fraction of the GP-I zone precipitates observed due to increasing alumina content in the cast composites used in the present study (Figure 12). Furthermore, as evident from the results of the resistivity measurements, solute diffusivity and hence precipitate growth rate are significantly enhanced due to the presence of reinforcements, at least at 473 K (Figure 8). Since both the β' and β peaks occur at temperatures well above 500 K (Figure 12), it is unlikely that slow solute diffusivity is responsible for the reduced volume fractions of these phases obtained in the present composites. Therefore, it is proposed that dislocation-aided strain relief *via* appropriate precipitate-dislocation orientation and the consequent stabilization of transition precipitates are responsible for the smaller volume fractions of the β' and β precipitates observed in the present MMCs.

Although both preaging and reinforcement addition reduce the vacancy concentration in the matrix, their effects on the aging behavior of the composite are very different. Both preaging and reinforcement addition result in the reduction of the volume fraction of silicon clusters formed during the DSC scan. However, while preaging increases the peak temperature (T_p) for silicon clustering, reinforcements have no effect on T_p. In addition, the presence of reinforcements increases the amount of GP-I zones, whereas preaging suppresses GP-I zone precipitation. While the primary effect of preaging is to slow nucleation by reducing the density of nucleation sites, the principal effects of reinforcement addition are to accelerate nucleation by reducing incubation time and enhance growth by providing numerous dislocations for pipe diffusion. Reinforcement addition is also expected to reduce the vacancy concentration in the matrix somewhat, although any effect of this on the precipitation behavior was found to be relatively small in the present materials.

V. CONCLUSIONS

The CTE mismatch between alumina and aluminum alloy 6061 results in a substantial increase of the matrix dislocation density due to the addition of 10 vol pct Al_2O_3 particulates. The addition of 15 vol pct alumina increased the dislocation density slightly more. Concurrent with this increased dislocation density, the time to peak hardness of the composites decreased with increasing reinforcement content.

Resistivity measurements revealed that the presence of alumina particulates accelerates both nucleation and growth of precipitates. Nucleation is enhanced primarily due to a reduction of the incubation time for silicon clustering, while growth is enhanced due to the increased solute diffusivity in the composite matrices. Both can be attributed to the increased density of thermally generated dislocations in the composites, which serve as sites for early nucleation and short circuit paths for solute diffusion.

Precipitate nucleation in the composite matrices was found to occur on two kinds of sites: dislocations generated as a result of the CTE mismatch between the matrix and the reinforcements and quenched-in vacancy loops. Only nucleation on the first type of sites was found to be accelerated. Reinforcement addition had little effect on the kinetics of nucleation at vacancy loops, as evident from the relatively constant peak temperature of the DSC exotherm for Si clustering.

Precipitate growth rate was found to be significantly accelerated, this acceleration being more evident for the more mature precipitates in the aging sequence (β' and β). This suggests that matrix dislocations appreciably enhance the diffusivity of magnesium in the matrix.

The addition of alumina reinforcements affects not only the precipitation kinetics, but also the relative amounts of the various phases present. Reinforcement addition was found to increase the volume fraction of GP-I zones while suppressing the formation of the β' and β phases. A plausible explanation is that because of the high dislocation density in the composites, the early precipitates, which are coherent with the matrix, can orient themselves relative to the dislocations so as to reduce the associated strain energy. This would stabilize these coherent precipitates and reduce the volume fraction of the semicoherent β' and incoherent β phases.

While both preaging and reinforcement addition decrease the vacancy concentration in the matrix and both result in the formation of some silicon clusters prior to aging, their effects on the precipitation behavior are significantly different. This suggests that the addition of alumina reinforcements has a more profound effect on the aging behavior of age hardenable aluminum matrix composites than just the acceleration of precipitation kinetics.

ACKNOWLEDGMENTS

This work was supported by funds administered by the Naval Postgraduate School Research Council. The authors would like to thank Professor T. Yamashita for his help with some of the TEM results. The authors are also grateful to Mr. William Hoover of Duralcan, United States, for supplying the cast composites used in this work.

REFERENCES

1. T.G. Nieh and R.F. Karlak: *Scripta Metall.*, 1984, vol. 18, p. 25.
2. R.J. Arsenault and R.M. Fisher: *Scripta Metall.*, 1983, vol. 17, p. 67.
3. I. Dutta, D.L. Bourell, and D. Latimer: *J. Comp. Matl.*, 1988, vol. 22, p. 829.
4. T. Christman, A. Needleman, S. Nutt, and S. Suresh: *Mater. Sci. Eng.*, 1989, vol. A107, p. 49.
5. I. Dutta and D.L. Bourell: *Mater. Sci. Eng.*, 1989, vol. A112, p. 67.
6. T. Christman and S. Suresh: *Acta Metall.*, 1988, vol. 36, p. 1691.
7. J.M. Papazian: *Metall. Trans. A*, 1988, vol. 19A, pp. 2945-53.
8. K.K. Chawla and M. Metzger: *J. Mater. Sci.*, 1972, vol. 7, p. 34.
9. M. Vogelsang, R.J. Arsenault, and R.M. Fisher: *Metall. Trans. A*, 1986, vol. 17A, pp. 379-89.
10. R.F. Arsenault and N. Shi: *Mater. Sci. Eng.*, 1986, vol. 81, p. 175.
11. I. Dutta and D.L. Bourell: *Acta Metall.*, 1990, vol. 38, p. 2041.
12. C.M. Friend and S.D. Luxton: *J. Mater. Sci.*, 1988, vol. 23, p. 3173.
13. S. Suresh, T. Christman, and Y. Sugimura: *Scripta Metall.*, 1989, vol. 23, p. 1599.
14. G. Duopuoy: in *Proc. 3rd Int. Conf. on HVEM*, P.R. Swann, C.J. Humphreys, and M.J. Goringe, eds., Academic Press, London, 1974, p. 427.
15. K.J. Hale and M. Henderson-Brown: *Micron*, 1973, vol. 4, p. 69.
16. I. Dutta and S.M. Allen: *J. Mater. Sci. Lett.*, 1991, vol. 10, p. 323.
17. E. Ozawa and H. Kimura: *Mater. Sci. Eng.*, 1971, vol. 8, p. 327.
18. I. Kovacs, J. Lendvai, and E. Nagy: *Acta Metall.*, 1972, vol. 20, p. 975.
19. S. Ceresara, E. Di Russo, P. Fiorini, and A. Giarda: *Mater. Sci. Eng.*, 1969–1970, vol. 5, p. 220.
20. W.F. Smith: *Metall. Trans.*, 1973, vol. 4, pp. 2435-40.
21. H. Cordier and W. Gruhl: *Z. Metallkd.*, 1965, vol. 56, p. 669.
22. H.J. Rack and R.W. Krenzer: *Metall. Trans. A*, 1977, vol. 8A, pp. 335-46.
23. G. Thomas: *J. Inst. Met.*, 1961–62, vol. 90, p. 57.
24. D.W. Pashley, J.W. Rhodes, and A. Sendorek: *J. Inst. Met.*, 1966, vol. 94, p. 41.
25. Y. Adda and J. Philibert: *La Diffusion dans les Solides*, University of France Press, Paris, 1966, vol. II, p. 1151.
26. M.H. Jacobs: *Phil. Mag.* 1972, vol. 26, p. 1.
27. P.A. Beaven, A.P. Davidson, and E.P. Butler: in *Proc. Int. Conf. on Solid-Solid Phase Transformations*, H.I. Aaronson, D.E. Laughlin, R.F. Sekerka, and C.M. Wayman, eds., TMS-AIME, 1982, p. 661.
28. A.A. Frost and R.G. Pearson: *Kinetics and Mechanisms*, John Wiley and Sons, New York, NY, 1961, p. 77.
29. P.N. Adler and R. DeIasi: *Metall. Trans. A*, 1977, vol. 8A, pp. 1185-90.
30. S.H. Lo, S. Dionne, G. Carpenter, and D. Zimcick: in *Interfaces in Metal-Ceramic Composites*, R.Y. Lin, R.J. Arsenault, G.P. Martins, and S.G. Fishman, eds., TMS-AIME, 1989, p. 165.